Catalysis Today xxx (2011) xxx–xxx

Contents lists available at ScienceDirect

Catalysis Today

journal homepage: www.elsevier.com/locate/cattod

Pd ensemble effects on oxygen hydrogenation in AuPd alloys: A combined density functional theory and Monte Carlo study

Hyung Chul Ham[a,1], J. Adam Stephens[a,1], Gyeong S. Hwang[a,*], Jonghee Han[b], Suk Woo Nam[b], Tae Hoon Lim[b]

[a] Department of Chemical Engineering, The University of Texas at Austin, Austin, TX 78712, United States
[b] Center for Fuel Cell Research, Korea Institute of Science and Technology, Seoul, Republic of Korea

ARTICLE INFO

Article history:
Received 28 September 2010
Received in revised form 14 January 2011
Accepted 8 February 2011
Available online xxx

Keywords:
PdAu alloy catalyst
Ensemble effect
Oxygen reduction reaction
Density functional theory
Cluster expansion method
Monte Carlo

ABSTRACT

Using density functional theory and cluster expansion-based Monte Carlo simulations, we examine the effect of Pd dispersion on the energetics and barriers for the reaction of O_2 with H atoms to form H_2O and H_2O_2 on a AuPd/Pd(1 1 1) alloy surface. Our calculations show that this hydrogenation reaction is considerably affected by the distribution of Pd and Au atoms in the surface layer. In particular, on isolated Pd monomers surrounded by less active Au atoms, the activation barrier to form H_2O_2 is appreciably lowered due to the suppression of O–O bond cleavage. In contrast, the reactivity to H_2O on the Pd dimer is predicted to be enhanced compared to pure Pd. Using Monte Carlo simulations we also predict Pd ensemble populations in the AuPd surface layer as a function of temperature and composition. Due to the favorability of Au–Pd interactions over Pd–Pd, we find that small ensembles, particularly monomers, preferentially exist. This study highlights how theoretical investigation of bimetallic alloys, particularly the surface arrangement of atoms and the influence of ensembles on reaction energetics, can offer insight into the design of catalysts and tailoring of reaction conditions.

1. Introduction

Low temperature PEM (polymer electrolyte membrane) fuel cells, also known as proton exchange membrane fuel cells, have received much attention in recent years as a promising alternative for power generation, especially for automotive applications. PEM fuel cells use hydrogen (or hydrogen-rich fuel) and oxygen (from air) to generate energy, thereby achieving near-zero pollutant emissions and high fuel efficiency [1]. One of the major barriers to their commercialization is the high cost arising largely from the use of expensive platinum (Pt)-containing electrocatalysts in the electrodes. In addition, the oxygen reduction reaction (ORR) at the cathode, in which molecular oxygen is decomposed and combined with protons and electrons supplied by the anode through the membrane and external circuit to form water, is currently the rate-limiting step for the PEM fuel cell. Pt-based catalysts are also susceptible to poisoning by carbon monoxide (CO) and other impurities [2]. For these reasons, there exists great interest in developing alternative catalyst materials.

One promising avenue is the use of palladium (Pd)-based bimetallic nanoparticles [3]. By itself, the activity of Pd toward the ORR has been found to be lower than that of Pt [3,4]. However, a series of recent experimental and theoretical studies have demonstrated that Pd alloyed with other metals (Fe, Co, Ni) has an ORR activity comparable to or even better than Pt catalysts [5–8]. The synergetic effect exhibited by Pd-containing and other bimetallic alloys can to a large extent be attributed to the existence of unique mixed-metal surface sites (the so called ensemble (geometric) effect [9–11]) and by electronic state change due to metal–metal interactions (the so called ligand (electronic) effect [12]). Knowledge of the arrangement of atoms in the surfaces of bimetallic catalysts is indispensable in elucidating the roles played by the ensemble and ligand effects in their activities. Although progress in this area has been hampered by the difficulty of atomic-scale characterization, computational approaches can be a powerful and flexible alternative.

In this article, we present the results of a density functional theory (DFT) study of the influence of Pd ensembles on the reactivity and selectivity of oxygen hydrogenation on the AuPd/Pd(1 1 1) surface. We also examine the effects of temperature and composition on the population of Pd ensembles in this surface using a Cluster Expansion Hamiltonian and the Monte Carlo method. We chose to examine the AuPd alloy because it has been found to possess significantly enhanced activity compared to monometallic Pd and Au

* Corresponding author.
E-mail address: gshwang@che.utexas.edu (G.S. Hwang).
[1] Both these authors contributed equally to this work.

0920-5861/$ – see front matter © 2011 Elsevier B.V. All rights reserved.
doi:10.1016/j.cattod.2011.02.006

catalysts for a host of reactions, such as direct synthesis of hydrogen peroxide (H_2O_2) from hydrogen (H_2) and oxygen (O_2) [11,13,14], hydrogen evolution [15] and production of vinyl acetate monomer [16–19]. This work is of value in understanding the nature of the effect of alloying on catalytic function, particularly in providing some insights into the performance of Pd-based alloy catalysts for the ORR.

2. Computational methods

2.1. Density functional theory

The calculations reported herein were performed on the basis of spin polarized density functional theory (DFT) within the generalized gradient approximation (GGA-PW91 [20]), as implemented in the Vienna Ab-initio Simulation Package (VASP) [21]. The projector augmented wave (PAW) method with a planewave basis set was employed to describe the interaction between core and valence electrons [22]. The valence configurations employed to construct the ionic pseudopotentials are as follows: $5d^{10}\ 6s^1$ for Au, $4d^9\ 5s^1$ for Pd, and $2s^2\ 2p^4$ for O. An energy cutoff of 350 eV was applied for the planewave expansion of the electronic eigen functions. For the Brillouin zone integration, we used a $(2 \times 2 \times 1)$ Monkhorst-Pack mesh of k points to calculate geometries and total energies, and increased the k-point mesh size up to $(7'7'1)$ to reevaluate corresponding electronic structures or to $(4'4'1)$ to refine the energies for construction of the Cluster Expansion Hamiltonian. Reaction pathways and barriers were determined using the nudged elastic band method (NEBM) with eight intermediate images for each elementary step [23].

For PdAu model surfaces, we constructed a four atomic-layer slab with either a rectangular $2\sqrt{3} \times 4$ (for surface reaction calculations) or a hexagonal 4×4 (for inclusion in the Cluster Expansion training set) unit cell in which a PdAu layer is overlaid on a three-layer Pd(1 1 1) slab with each layer composed of 16 atoms. The slab is separated from its periodic images in the vertical direction by a vacuum space corresponding to seven atomic layers. The lattice constant for bulk Pd is predicted to be 3.95 Å (this is in accordance with a DFT result of 3.96 Å [24]), close to the experimental value of 3.89 Å. While the bottom two layers of the four-layer slab were fixed at corresponding bulk positions, the upper two layers were fully relaxed using the conjugate gradient method until residual forces on all the constituent atoms become smaller than $5'10^{-2}$ eV/Å. The adsorption energy (E_{ad}) is calculated by $E_{ad} = |E(\text{adsorbate}/M)| - |E(M) + E(\text{adsorbate})|$, where E(adsorbate/M), $E(M)$, and E(Adsrobate) represent the total energies of the adsorbate/slab system, the slab, and an isolated adsorbate molecule in the gas state, respectively, and $|x|$ indicates the absolute value of x.

2.2. Cluster expansion method

DFT is an established method of predicting the structure and energies of metallic alloys. However, due to its computational expense, the practical application of DFT usually is limited to sampling a small number of configurations containing on the order of 100 atoms. By contrast, when Monte Carlo (MC)-based simulation schemes are used to obtain thermodynamic averages, it is not uncommon to sample, on a per atom basis, thousands of microstates. To bridge the gap between highly accurate but expensive higher order methods like DFT and the sampling requirements of MC simulation, it is necessary to use a model Hamiltonian. Hamiltonians constructed using the Cluster Expansion (CE) method have been shown to be capable of reproducing DFT-predicted energies to within a few meV per atom in crystalline materials [25–31].

In the CE method, each lattice site in a binary, crystalline alloy is assigned a spin corresponding to the chemical species that occupies it (i.e., for Au and Pd, $s = +1$ and -1, respectively), and then the energy of the lattice is expanded in terms of clusters of these spins, which form a complete basis. That is,

$$E(\hat{S}) = J_0 + \sum_i J_i s_i + \sum_{i<j} J_{ij} s_i s_j + \sum_{i<j<k} J_{ijk} s_i s_j s_k + \cdots$$

where J_o, J_i, J_{ij}, and J_{ijk} are the interaction coefficients (called *effective cluster interactions* (ECIs)) for the empty, point, pair, and three body spin clusters, and s_i is the spin (± 1) of lattice site i. In practice, cluster expansions can be truncated to just a few terms without a great loss of fidelity.

In our model of the fcc (1 1 1) surface, the 2D hexagonal lattice, we distinguish between *hcp* 3-fold hollow sites, which are situated directly above an atom in the first subsurface layer, and fcc 3-fold hollow sites, which are not. We chose to limit the range of interactions in our expansion to the third nearest neighbor distance. Thirty-six unique types of clusters, capable of forming 2^{36} ($\sim 6.9 \times 10^{10}$) possible cluster expansions, fit this criterion.

We used the cross validation (CV) score [32], which is a measure of the prediction error of a model, to select one cluster expansion from among these possibilities. A global optimization technique called simulated annealing [33] was used to determine the set of clusters that minimized the CV score with respect to a training set of DFT-predicted energies. The initial training set contained 30 model surfaces, but to help guard against the possibility of bias, the set was iteratively expanded during the cluster selection process [32,34]. In each iteration, a cluster expansion was created from the training set using simulated annealing. Then, this CE was used to generate new ground-state model surfaces. Finally, the surfaces were added to the training set if not already present. Convergence was achieved when the newly generated CE predicted no new ground-state configurations. This procedure is explained in greater detail elsewhere [12].

With our cluster expansion in hand, we performed Monte Carlo simulations [35] on the AuPd surface alloy for a range of compositions and temperatures. In each sampling step, a new configuration was generated by swapping randomly chosen Au and Pd atoms. Using these simulations, we calculated the average number of Pd monomers and dimers at each condition; the results are presented in Section 3.3.

3. Results and discussion

3.1. Oxygen reduction reaction: mechanism overview

The oxygen reduction reaction (ORR) is a four-electron process involving the activation and conversion of molecular oxygen (O_2) to water (H_2O) (Eq. (1)). Catalysts with poor ORR activity can convert the O_2 instead to hydrogen peroxide (H_2O_2) by a two-electron reduction reaction as shown in Eq. (2).

$$O_2 + 4H^+ + 4e^- = 2H_2O \quad (1)$$

$$O_2 + 2H^+ + 2e^- = H_2O_2 \quad (2)$$

H_2O_2 is largely responsible for membrane deterioration in PEM fuel cells, accordingly degrading device performance. Therefore, suppression of H_2O_2 formation is a critical goal in catalyst design. At the same time, even if the catalyst shows high selectivity for H_2O production, it is possible that the H_2O formation rate is slow due to a high kinetic barrier in the relevant H_2O production path. A second design goal should be to reduce the barrier of the rate-determining step in order to enhance the reaction rate for H_2O formation.

In what follows, we report the effect of Pd ensembles in the AuPd/Pd(1 1 1) surface layer on H_2O formation reactivity and selec-

Please cite this article in press as: H.C. Ham, et al., Pd ensemble effects on oxygen hydrogenation in AuPd alloys: A combined density functional theory and Monte Carlo study, Catal. Today (2011), doi:10.1016/j.cattod.2011.02.006

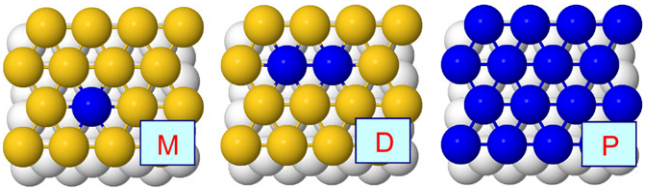

Fig. 1. Top views of the model PdAu surfaces considered in this work: Pd monomer (indicated as M), dimer (D), and pure (P). The black (blue), grey (gold), and white balls represent surface Pd, surface Au, and subsurface Pd atoms, respectively. (For interpretation of the references to color in this figure legend, the reader is referred to the web version of the article.)

tivity. We evaluated two different Pd ensembles, the monomer (indicated by M throughout the paper) and dimer (D), and compared them to the pure (1 1 1) surface (P); all shown in Fig. 1. The H_2O/H_2O_2 formation pathways that we examined are illustrated in Fig. 2, in which the nodes represent quasi-stable reaction intermediates and the paths between them indicate either hydrogenation (denoted +H) or O–O bond scission. Note that H atoms are supplied by H_2 oxidation at the anode in a PEM fuel cell.

Here, the H_2O formation pathways are classified by the behavior of O_2 absorbed on the catalyst surface. In dissociative pathways (I and II), adsorbed O_2 first undergoes bond scission, while in associative pathways (III, IV, V), it is directly hydrogenated to form OOH [4]. In pathway I, H_2O is produced from dissociated O_2 by two successive hydrogenation steps, and in pathway II, two OH (resulting from hydrogenation of O radicals) combine to form H_2O. In the associative pathways, the adsorbed OOH radical either splits to form O + OH before merging with pathway I (pathway III) or pathway II (pathway IV), or it undergoes a second hydrogenation to form H_2O_2 (pathway V) which either desorbs or splits into OH + OH prior to H_2O formation. In the following section, we examine these pathways in terms of reaction energies (that is, the difference in energy of adjacent nodes) and activation barriers (to transition from one node to the next) for the pure Pd surface and the Pd monomer and dimer sites.

All calculations were performed in the gas phase rather than in a solution environment; however, we expect that the solution contributions to the surface reaction energetics and pathways would not be significant considering that the weak electrostatic interactions such as hydrogen bonding between adsorbed reactants and intermediates (such as O_2 and OOH) and solution species (such as H_2O) can be much weaker than the interaction of the reactants/intermediates with the metal alloy surfaces considered [4].

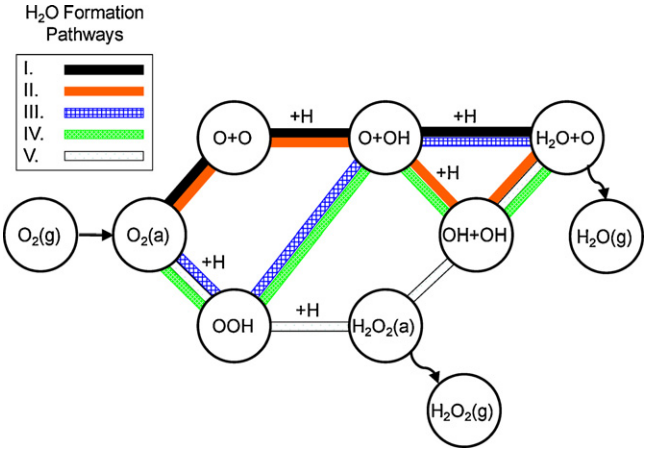

Fig. 2. Schematic illustration of H_2O/H_2O_2 formation steps considered in this study.

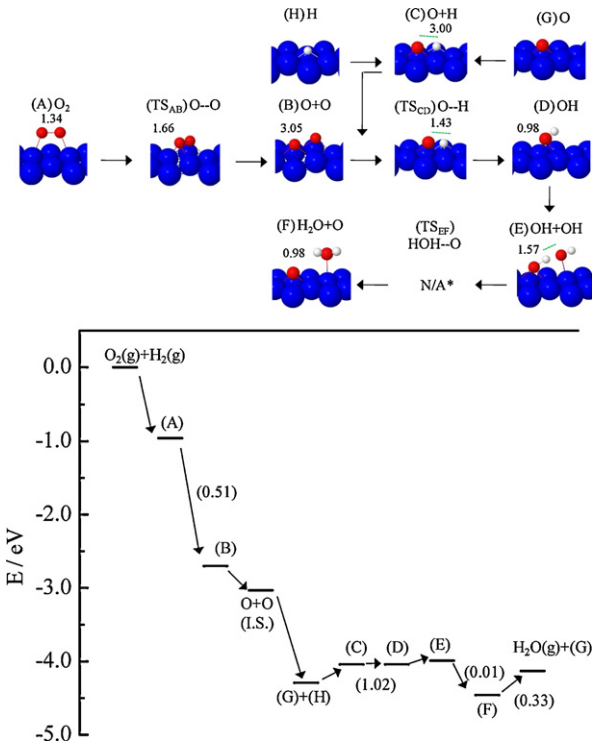

Fig. 3. Predicted potential energy diagram for H_2O formation from H and O_2 on Pd(1 1 1), and corresponding intermediate and transition state configurations. In the energy diagram (lower panel), the activation energies for the hydrogenation, scission, and desorption reactions considered are given in eV, and I.S. refers to the infinite separation of two adsorbates. On Pd(1 1 1), our calculation shows that the hydrogenation of OOH leads to nearly spontaneous dissociation into OH + OH, i.e., OOH + H → OH + OH; thus, no activation energy was obtained for the hydrogenation reaction, as indicated by N/A. In the intermediate and transition states, the O–H and O–O distances are indicated in the hydrogen and scission reactions, respectively. The big black (blue), small dark grey (red), and small white balls represent Pd, O, and H atoms, respectively. (For interpretation of the references to color in this figure legend, the reader is referred to the web version of the article.)

3.2. H_2O versus H_2O_2 formation: pathways and energetics

3.2.1. Pure Pd(1 1 1)

Fig. 3 shows the energy changes and activation barriers in relevant reaction paths for H_2O formation on the pure Pd(1 1 1) surface; in Table 1, we also summarize the energetics and barriers involved in the hydrogenation and scission reactions leading to either H_2O or H_2O_2 formation. Our results suggest that the formation of H_2O would preferentially follow the dissociative mechanism, as the O_2 dissociation barrier is much lower, by 0.38 eV, than the O_2 hydrogenation barrier. The following O hydrogenation is predicted to be

Table 1
Calculated total energy changes (ΔE) and activation barriers (E_a in parentheses) for hydrogenation and decomposition reactions. All energy values are given in eV.

	$AuPd_M$/ Pd(1 1 1)	$AuPd_D$/ Pd(1 1 1)	P
(A) $O_2 + H \rightarrow OOH$	−0.73 (0.53)	−0.25(0.84)	0.18 (0.89)
(A) $O_2 \rightarrow O + O$	0.25 (1.55)	−0.23 (1.54)	−2.08 (0.51)
(B) $OOH + H \rightarrow H_2O_2$	−0.86 (0.37)	−0.51 (0.81)	0.09 (–)[a]
(B)′ $OOH \rightarrow O + OH$	−0.39 (0.81)	−0.92 (0.54)	−2.13 (0.31)
(C) $H_2O_2 \rightarrow H_2O_2(g)$	0.17 (0.17)	0.18 (0.18)	0.24 (0.24)
(C)′ $H_2O_2 \rightarrow OH + OH$	−0.90 (0.31)	−1.35 (0.11)	−2.09 (0.01)
(D) $O + H \rightarrow OH$	−1.37 (0.67)	−0.94 (0.80)	0.13 (1.15)
(F) $OH + H \rightarrow H_2O$	−1.44 (0.45)	−0.99 (0.85)	−0.27 (0.95)
(G) $OH + OH \rightarrow H_2O + O$	−0.17 (0.14)	0.11 (0.19)	−0.43 (0.05)

[a] The OOH hydrogenation results in almost spontaneous HO–OH dissociation with no sizable barrier, i.e., OOH + H → OH + OH.

Please cite this article in press as: H.C. Ham, et al., Pd ensemble effects on oxygen hydrogenation in AuPd alloys: A combined density functional theory and Monte Carlo study, Catal. Today (2011), doi:10.1016/j.cattod.2011.02.006

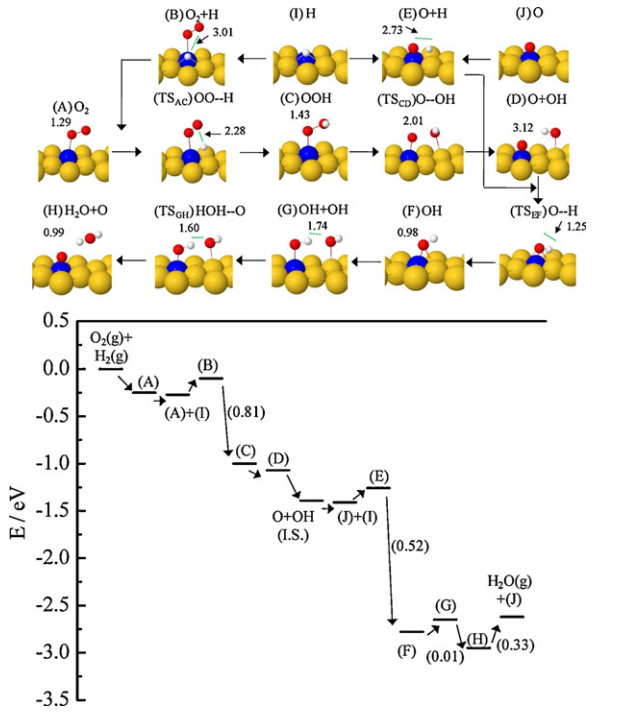

Fig. 4. Predicted potential energy diagram for direct for H_2O formation from H and O_2 at the Pd monomer site, and corresponding intermediate and transition state configurations. In the energy diagram (lower panel), the activation energies for the hydrogenation, scission, and desorption reactions considered are given in eV, and I.S. refers to the infinite separation of two adsorbates. In the intermediate and transition states, the O–H and O–O distances are indicated in the hydrogen and scission reactions, respectively. The big grey (yellow) and black (blue) balls represent surface Au and Pd atoms, respectively, and the small dark grey (red) and white balls indicate O and H atoms, respectively. (For interpretation of the references to color in this figure legend, the reader is referred to the web version of the article.)

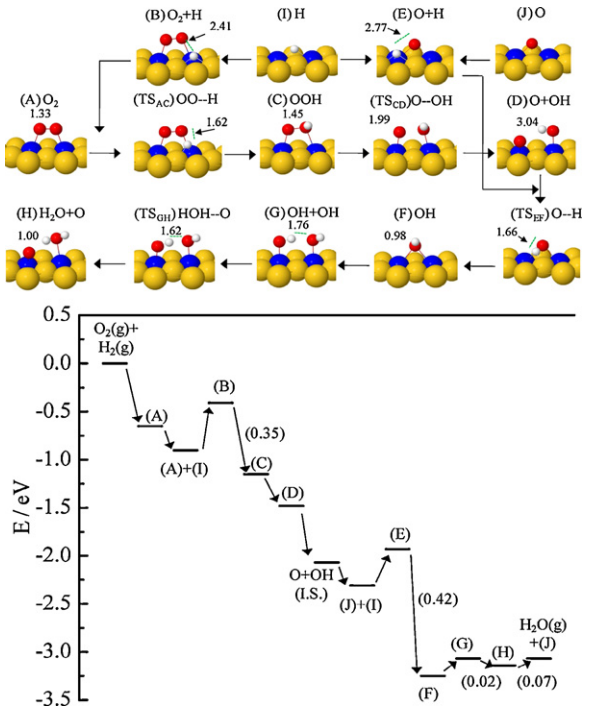

Fig. 5. Predicted potential energy diagram for H_2O formation from H and O_2 at the Pd dimer site, and corresponding intermediate and transition state configurations. In the energy diagram (lower panel), the activation energies for the hydrogenation, scission, and desorption reactions considered are given in eV, and I.S. refers to the infinite separation of two adsorbates. In the intermediate and transition states, the O–H and O–O distances are indicated in the hydrogen and scission reactions, respectively. The big grey (yellow) and black (blue) balls represent surface Au and Pd atoms, respectively, and the small dark grey (red) and white balls indicate O and H atoms, respectively. (For interpretation of the references to color in this figure legend, the reader is referred to the web version of the article.)

endothermic ($\Delta E = 0.13$ eV) with a barrier of 1.15 eV. In the final step, H_2O can be formed by two different reactions: OH hydrogenation (pathway I) or OH + OH combination (pathway II). The OH hydrogenation is calculated to be exothermic by 0.27 eV and has a barrier of 0.95 eV. In contrast, the OH + OH combination reaction has much smaller barrier (0.05 eV), implying that pathway II is the energetically preferred route for H_2O formation on pure Pd(1 1 1). The highest barrier occurs at the O hydrogenation step, with a height of 1.15 eV.

3.2.2. Pd monomer in AuPd/Pd(1 1 1)

For the monomer case, as shown in Fig. 4 we find that H_2O formation tends to occur via an associative mechanism. According to our calculations, O_2 hydrogenation has a much lower barrier (0.53 eV) than O_2 dissociation (1.55 eV). The barrier for OOH hydrogenation is 0.37 eV, also considerably lower than the O + OH scission barrier of 0.81 eV. This suggests that the reaction at the monomer site may proceed along pathway V until H_2O_2 is produced, assuming that H atoms are readily available. However, H_2O_2 desorption has a lower barrier than OH + OH scission (0.17 eV versus 0.31 eV), which might indicate that the monomer is a poor surface site for H_2O formation from H and O_2. Indeed, recent theoretical studies [11] have demonstrated that isolated Pd monomers surrounded by less active Au atoms are primarily responsible for the significantly enhanced selectivity in the direct synthesis of H_2O_2 from H_2 and O_2 by suppressing O–O bond cleavage. Here, we should point out that identification of the monomer as a poor catalyst site for H_2O formation depends on the assumption that H atoms are readily available on the cathode surface. If, despite the difference in their barriers, hydrogenation occurs more slowly than O–O (or O–OH) scission due to a scarcity of H, H_2O selectivity on the monomer may improve (Fig. 5).

An explanation for this dramatic change of selectivity on the Pd monomer compared to the pure Pd(1 1 1) surface is suggested by differences in the adsorption energies of the reaction intermediates. Compared to the Pd monomer, the pure Pd(1 1 1) surface stabilizes the O/OH/H radicals much more than OOH/H_2O_2. Specifically, for O/OH/H (at a hollow site for (O/H) and at a top site for (OH)), the adsorption energies are 3.43/1.68/2.29 eV (M) and 4.95/2.31/2.90 eV (P), while for OOH/H_2O_2, they are 0.89/0.17 eV (M) and 1.30/0.24 eV (P). In the reaction pathways illustrated in Fig. 2, these two sets of species are coupled to one another as reactant/product pairs through either hydrogenation or O–O bond scission. Unequal adsorption energy changes in reactants and products on the pure surface versus the monomer provides an explanation for the energetic preference of one reaction pathway (and final product) over another, provided that the activation barriers are directly related to the relative stabilities of the reactants and products.

3.2.3. Pd dimer in AuPd/Pd(1 1 1)

For the dimer case, O_2 reduction may follow an associative mechanism as in the monomer case. The barrier for O_2 dissociation is larger by 0.70 eV than for O_2 hydrogenation. However, unlike the monomer case, pathway V is unfavorable, as O–O bond scission to form O + OH has a lower barrier (0.54 eV) than hydrogenation to form H_2O_2 (0.81 eV). Since the barrier changes are connected to the relative binding strength between OOH/H_2O_2 and dissociated O/OH/H radicals, we compared their binding energies. As summa-

Please cite this article in press as: H.C. Ham, et al., Pd ensemble effects on oxygen hydrogenation in AuPd alloys: A combined density functional theory and Monte Carlo study, Catal. Today (2011), doi:10.1016/j.cattod.2011.02.006

Table 2
Calculated binding energies (in eV) of O, H, OH, OOH and H_2O_2 at a hollow site (for O/H) and at a top site (for OH/OOH/H_2O_2).

	$AuPd_M$/Pd(1 1 1)	$AuPd_D$/Pd(1 1 1)	P
O	3.43	3.87	4.95
OH	1.68	2.05	2.31
H	2.29	2.51	2.90
OOH	0.89	1.03	1.30
H_2O_2	0.17	0.18	0.24

rized in Table 2, the adsorption energies of O/OH on the dimer (3.87/2.05 eV) are noticeably increased compared to the monomer case (3.43/1.68 eV). In contrast, the variation of OOH adsorption energy is relatively small, i.e., 1.03 eV (D) and 0.89 eV (M). Accordingly, O + OH scission exothermicity increases from 0.39 eV (M) to 0.92 eV (D) and in turn the barrier substantially reduces from 0.81 eV (M) to 0.54 eV (D). On the other hand, in the OOH hydrogenation case, increases in the adsorption energies of the reactants H/OOH (2.29/0.89 eV (M) → 2.51/1.03 eV (D)) are large compared to changes in H_2O_2 binding (0.17 eV (M) → 0.18 eV (D)), which partially explains an increase in the barrier from 0.37 eV (M) to 0.81 eV (D).

In the next O hydrogenation step, our calculation predicts an exothermicity of 0.94 eV and a barrier of 0.80 eV, indicating that the O hydrogenation reaction on the dimer can occur more easily than in the pure Pd(1 1 1) case. Note that the reaction on the pure Pd(1 1 1) surface is endothermic by 0.13 eV and the barrier is 1.15 eV.

In OH hydrogenation, we calculated the barrier to be 0.85 eV, which is slightly lower by 0.10 eV than on the pure Pd(1 1 1) surface. On the other hand, in the OH + OH combination reaction, the barrier is predicted to be 0.19 eV, indicating that OH hydrogenation is more difficult than OH + OH combination. Therefore, the energetically preferred H_2O formation route on the Pd dimer is likely reaction pathway IV with a maximum barrier of 0.80 eV at O_2 hydrogenation. On the pure Pd(1 1 1) surface, the maximum barrier was 1.15 eV, which suggests that the presence of Pd dimers may improve the formation rate of H_2O.

This enhancement of H_2O formation rate comes from the reduced surface reactivity toward adsorbates. It has been previously reported [4,36] that surfaces which strongly bind adsorbates such as O/OH tend to reduce the rate of water formation by retarding O/OH hydrogenations, while for surfaces which weakly bind adsorbates, the opposite is true (provided that the O–O scission barrier is not increased too much).

For the pure Pd surface, the ability to bind adsorbates is relatively strong compared to the pure Pt surface. Since the rate-determining step in H_2O formation on the Pt catalyst is believed to be the O/OH hydrogenation steps, the increase of surface reactivity on the Pd catalyst gives rise to a reduction in the kinetics of the H_2O formation by further suppressing the O/OH hydrogenation reaction. However, the creation of small Pd ensembles (such as dimers) by alloying Pd with Au atoms reduces the surface reactivity toward the adsorbate, resulting in a decrease of the adsorption energy of adsorbates like O/OH (see Table 2). This results in a reduction of the barriers for O/OH hydrogenation compared to the pure Pd(1 1 1) surface without significantly changing the O–O bond scission barrier as shown in the previous section. In contrast, on the monomer, the adsorbate is not activated sufficiently to break the O–O bond and the H_2O_2 is selectively formed, resulting in the degradation of fuel cell materials. These results suggest that one of the challenges of designing a AuPd catalyst for use in the fuel cell cathode is increasing the population of small ensembles while simultaneously suppressing the formation of monomers. Alternatively, as we pointed out earlier, it might be possible to minimize evolution of the by-product (H_2O_2) by reducing H atom coverage on the cathode catalyst surface in order to decrease the rate of OOH hydrogenation at monomer sites.

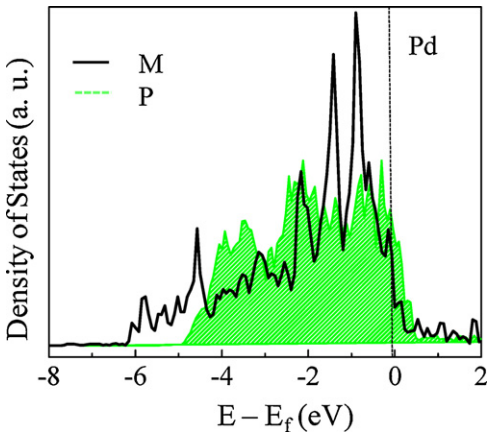

Fig. 6. Density of states projected on the outmost *d*-states of the Pd monomer (M) and pure surface (P). The dotted line indicates the Fermi level position.

3.3. Pd ensembles in AuPd/Pd(1 1 1): formation and distribution

Having considered how the kinetics of oxygen hydrogenation are influenced by different Pd ensembles in the AuPd/Pd(1 1 1) surface, we are confronted by an important question: how are the Au and Pd atoms actually arranged in real catalyst particles? To begin to answer this question, we first examined the interaction between Au and Pd atoms in the AuPd/Pd(1 1 1) surface. Next, we used our Cluster Expansion Hamiltonian and the Monte Carlo simulation scheme to predict the effects of temperature and Pd coverage (θ, in atomic percent) on the populations of monomers and dimers in the AuPd/Pd(1 1 1) surface.

3.3.1. Au–Pd interaction: DFT calculations

Using DFT, we calculated that the formation energies per Pd atom (E_f) of the Pd monomer and dimer are 0.07 eV and 0.11 eV, respectively, as given by: $E_f = [E_{PdAu} - E_{Au} + N_{Pd}(E_{Au\text{-}bulk} - E_{Pd\text{-}bulk})]/N_{Pd}$, where E_{PdAu}, E_{Au}, $E_{Au\text{-}bulk}$, and $E_{Pd\text{-}bulk}$ refer to the total energies of the PdAu/Pd(1 1 1) slab, Au/Pd(1 1 1) slab, bulk Au (per atom), and bulk Pd (per atom), respectively, and N_{Pd} indicates the number of Pd atoms on a given PdAu surface. This implies that Pd would have a tendency to remain isolated, rather than forming aggregates in the AuPd surface alloy.

Fig. 6 shows the local density of states (LDOS) projected onto the *d*-bands of a Pd monomer in the AuPd surface alloy and the pure Pd(1 1 1) surface. The LDOS of the Pd monomer noticeably broadens as compared to the Pd(1 1 1) case; in particular, the onset of the high binding energy tail shifts down below −6 eV (from around −5 eV in Pd(1 1 1)) while the peaks near the Fermi level ($-1\text{ eV} < E - E_f$) appear to be reduced. In addition, the *d*-band center of the monomer is 0.07 eV lower than that of Pd(1 1 1). These results suggest that the heteronuclear Au–Pd interaction is stronger than the homonuclear Pd–Pd interaction, and also help explain the reduced reactivity at the monomer site compared to pure Pd(1 1 1).

3.3.2. Pd ensemble distribution: MC simulations

Fig. 7 shows results from MC simulations; behavior in the high ("infinite") temperature limit, where atomic interactions are negligible, is represented by the random alloy. At infinite temperature, the fraction of surface Pd atoms that exist as monomers (Fig. 7(a)) monotonically decreases with increasing coverage. This is a consequence of the fact that when the surface contains few Pd atoms,

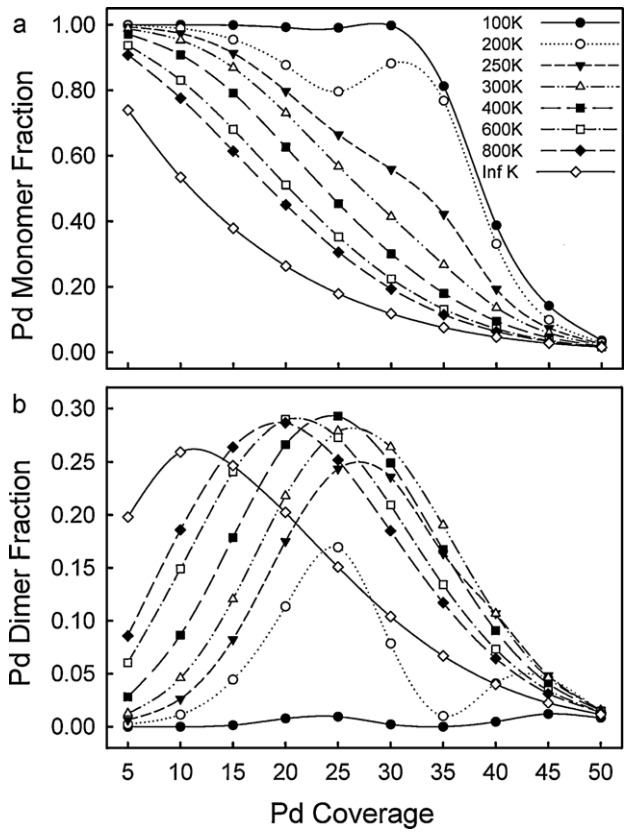

Fig. 7. Average fraction of surface Pd atoms in monomers (a) and dimers (b) in AuPd surface alloys at several levels of Pd coverage and temperature.

the probability of finding two or more together is low, but as the surface becomes more crowded, it increases. Unlike the monomer plot, the infinite temperature dimer plot (Fig. 7(b)) passes through a maximum at approximately $\theta = 12\%$. As more Pd atoms crowd the surface, the probability of randomly placing two together increases. This explains the initial rise. However, the same is true of trimers, tetramers, and other, larger ensembles. The fraction of Pd atoms in dimers must at some point give way to the growing fraction in larger ensembles and begin to diminish.

The overall shape of most of the finite temperature Pd monomer plots (Fig. 7(a)) resembles the infinite temperature limit. The $T = 100$ K and 200 K plots are exceptions. The maxima they exhibit at $\theta = 30$–35% can be attributed to the stability of the $(\sqrt{3} \times \sqrt{3})R30^\circ$ ordered phase [37]. This surface, which is the ground state for a Pd coverage of 1/3, is unique to two other ways: (i) it is the only one with a coverage of 1/3 in which all Pd atoms can exist as monomers and (ii) no such surfaces exist at Pd coverage >1/3.

Regardless of temperature, at $\theta = 5\%$, between 74% and 100% of Pd atoms are monomers, but at $\theta = 50\%$, fewer than 4% are. As expected, reducing the temperature (thereby increasing the contribution of interatomic interactions) results in a significant enhancement of the monomer population at all levels of coverage. At $\theta = 30\%$ and $T = 100$ K, close to 100% of Pd atoms exist as monomers, while at $T = \infty$, only around 12% do. Even at 800 K, the monomer fraction differs from the random model by as much as 24 percentage points (at $\theta = 10\%$).

Plots of the Pd dimer fractions (Fig. 7(b)) at the finite temperatures considered exhibit maxima, just as at infinite temperature. However, relative to the random alloy, the maxima are shifted increasingly toward higher coverage as temperature decreases. The shift is equal to about 15 percentage points in the $T = 250$ K case. This is apparently due to the preference for small ensembles in the AuPd surface alloy. The preference for monomers over dimers delays the rise of the dimer fraction, and decline of the dimer fraction likewise is delayed by the preference for dimers over larger ensembles. Due to the $(\sqrt{3} \times \sqrt{3})R30^\circ$ ordered surface, the $T = 100$ K and 200 K dimer plots have minima at $\theta = 30$–35% that coincide with the previously mentioned maxima in the monomer plots.

4. Conclusions

Spin-polarized DFT calculations were performed to examine the effect of Pd ensembles on the reaction of O_2 with H atoms to form H_2O and H_2O_2 on a AuPd alloy surface. Our calculations show that the energetics and barriers of the reduction reactions can be considerably affected by the distribution of Pd and Au atoms in the surface layer. The most energetically favored reaction pathway at a Pd monomer site results in the formation of H_2O_2 due to the suppression of O–O bond cleavage; this might indicate that it is a poor site for H_2O formation especially if H atoms are readily available. On the other hand, on the Pd dimer, H_2O tends to be the preferred product. We calculate that the maximum activation barrier for H_2O formation on the dimer is lower than for the pure Pd(1 1 1) surface by about 0.35 eV as a result of reduced hydrogenation barriers. At the less active small Pd ensemble sites, the binding energies of O, OH and H are significantly lowered compared to the pure Pd(1 1 1) surface, which in turns facilitates the hydrogenation reactions leading to H_2O. This suggests that an AuPd alloy with a large population of small ensembles (such as dimers) and few monomers in its surface might be beneficial for the ORR. However, according to our Monte Carlo simulations of the AuPd surface alloy, monomers are the dominant Pd ensemble for a wide range of temperatures and compositions, mainly attributed to the preference in the AuPd surface for the heteronuclear Pd–Au interaction. Hence, to improve H_2O selectivity on a AuPd alloy surface, one potential strategy might be to limit the surface coverage of H atoms, thereby slowing the kinetics of OOH hydrogenation and increasing O + OH scission. It is also possible that larger Pd ensembles could be induced to form in the surface by adsorbates, which in turn might improve H_2O selectivity. For example, our calculations indicate that with the addition of a single adsorbed O atom, the Pd dimer becomes around 0.4 eV more stable than a pair of isolated monomers. This effect will be more fully explored in later studies. These findings show how a combined DFT and Monte Carlo study of the surface ensembles and their effects on surface chemistry can offer insight into the design of bimetallic catalysts and tailoring of reaction conditions.

Acknowledgements

This work was supported by the R. A. Welch Foundation (F-1535). The authors also thank the Texas Advanced Computing Center for use of their computing resources.

References

[1] V. Wolf, A. Lamm, H.A. Gasteiger, Handbook of fuel cells, in: Electrocatalysis, vol. 2, John Wiley & Sons Ltd., 2003.
[2] M.H. Shao, T. Huang, P. Liu, J. Zhang, K. Sasaki, M.B. Vukmirovic, R.R. Adzic, Langmuir 22 (2006) 10409–10415.
[3] E. Antolini, Energy Environ. Sci. 2 (2009) 915–931.
[4] J.K. Norskov, J. Rossmeisl, A. Logadottir, L. Lindqvist, J.R. Kitchin, T. Bligaard, H. Jonsson, J. Phys. Chem. B 108 (2004) 17886–17892.
[5] M.H. Shao, P. Liu, J.L. Zhang, R. Adzic, J. Phys. Chem. B 111 (2007) 6772–6775.
[6] J.L. Fernandez, V. Raghuveer, A. Manthiram, A.J. Bard, J. Am. Chem. Soc. 127 (2005) 13100–13101.
[7] Y.G. Suo, L. Zhuang, J.T. Lu, Angew. Chem. Int. Ed. 46 (2007) 2862–2864.
[8] M.H. Shao, K. Sasaki, R.R. Adzic, J. Am. Chem. Soc. 128 (2006) 3526–3527.
[9] P. Liu, J.K. Norskov, Phys. Chem. Chem. Phys. 3 (2001) 3814–3818.
[10] H.C. Ham, G.S. Hwang, J. Han, S.W. Nam, T.H. Lim, J. Phys. Chem. C 114 (2010) 14922–14928.

Please cite this article in press as: H.C. Ham, et al., Pd ensemble effects on oxygen hydrogenation in AuPd alloys: A combined density functional theory and Monte Carlo study, Catal. Today (2011), doi:10.1016/j.cattod.2011.02.006

[11] H.C. Ham, G.S. Hwang, J. Han, S.W. Nam, T.H. Lim, J. Phys. Chem. C 113 (2009) 12943–12945.
[12] J.A. Stephens, H.C. Ham, G.S. Hwang, J. Phys. Chem. C 114 (2010) 21516–21523.
[13] J.K. Edwards, A.F. Carley, A.A. Herzing, C.J. Kiely, G.J. Hutchings, Faraday Discuss. 138 (2008) 225–239.
[14] S. Abate, G. Centi, S. Melada, S. Perathoner, F. Pinna, G. Strukul, Catal. Today 104 (2005) 323–328.
[15] Y. Pluntke, L.A. Kibler, D.M. Kolb, Phys. Chem. Chem. Phys. 10 (2008) 3684–3688.
[16] E.G. Allison, G.C. Bond, Catal. Rev. 7 (1972) 233–289.
[17] M.S. Chen, D. Kumar, C.W. Yi, D.W. Goodman, Science 310 (2005) 291–293.
[18] C.W. Yi, K. Luo, T. Wei, D.W. Goodman, J. Phys. Chem. B 109 (2005) p18535–18540.
[19] F. Maroun, F. Ozanam, O.M. Magnussen, R.J. Behm, Science 293 (2001) 1811–1814.
[20] J.P. Perdew, Y. Wang, Phys. Rev. B 45 (1992) 13244–13249.
[21] G. Kresse, J. furthmuller, VASP the Guide, Vienna University of Technology, Vienna, Austria, 2001.
[22] P.E. Blochl, Phys. Rev. B 50 (1994) 17953–17979.
[23] G. Henkelman, B.P. Uberuaga, H. Jonsson, J. Chem. Phys. 113 (2000) 9901–9904.
[24] A. Eichler, F. Mittendorfer, J. Hafner, Phys. Rev. B 62 (2000) 4744–4755.
[25] S.V. Barabash, V. Blum, S. Muller, A. Zunger, Phys. Rev. B 74 (2006) 035108.
[26] V. Blum, A. Zunger, Phys. Rev. B 70 (2004) 155108.
[27] V. Blum, A. Zunger, Phys. Rev. B 69 (2004) 020103.
[28] J.W.D. Connolly, A.R. Williams, Phys. Rev. B 27 (1983) 5169–5172.
[29] L.G. Ferreira, S.H. Wei, A. Zunger, Phys. Rev. B 40 (1989) 3197–3231.
[30] D.B. Laks, L.G. Ferreira, S. Froyen, A. Zunger, Phys. Rev. B 46 (1992) 12587–12605.
[31] K. Yuge, A. Seko, A. Kuwabara, F. Oba, I. Tanaka, Phys. Rev. B 76 (2007) 045407.
[32] A. van de Walle, G. Ceder, J. Phase Equilbr. 23 (2002) 348–359.
[33] M.J. Quinn, Parallel Programming in C with MPI and Open MP, McGraw-Hill, New Delhi, 2004.
[34] A. Zunger, L.G. Wang, G.L.W. Hart, M. Sanati, Model. Simulat. Mater. Sci. Eng. 10 (2002) 685–706.
[35] D. Frenkel, B. Smit, Understanding Molecular Simulation: From Algorithms to Applications, Academic Press, San Diego, 1996.
[36] J.L. Zhang, M.B. Vukmirovic, Y. Xu, M. Mavrikakis, R.R. Adzic, Angew. Chem. Int. Ed. 44 (2005) 2132–2135.
[37] J.A. Boscoboinik, C. Plaisance, M. Neurock, W.T. Tysoe, Phys. Rev. B 77 (2008) 045422.

Please cite this article in press as: H.C. Ham, et al., Pd ensemble effects on oxygen hydrogenation in AuPd alloys: A combined density functional theory and Monte Carlo study, Catal. Today (2011), doi:10.1016/j.cattod.2011.02.006